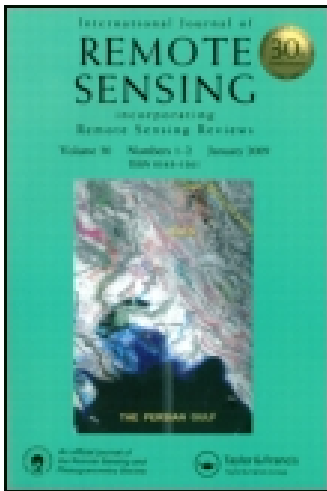


This article was downloaded by: [European Space Agency]

On: 30 July 2014, At: 03:33

Publisher: Taylor & Francis

Informa Ltd Registered in England and Wales Registered Number: 1072954 Registered office: Mortimer House, 37-41 Mortimer Street, London W1T 3JH, UK



International Journal of Remote Sensing

Publication details, including instructions for authors and subscription information:

<http://www.tandfonline.com/loi/tres20>

The PROBA-V mission: image processing and calibration

Sindy Sterckx^a, Iskander Benhadj^a, Geert Duhoux^a, Stefan Livens^a, Wouter Dierckx^a, Erwin Goor^a, Stefan Adriaensen^a, Walter Heyns^a, Kris Van Hoof^a, Gert Strackx^a, Kris Nackaerts^a, Ils Reusen^a, Tanja Van Achteren^a, Jan Dries^a, Tom Van Roey^a, Karim Mellab^b, Riccardo Duca^b & Joe Zender^b

^a Flemish Institute for Technological Research (VITO) - Remote Sensing Unit, Noordwijk, The Netherlands

^b ESA-ESTEC, Keplerlaan 1, Noordwijk, The Netherlands

Published online: 27 Mar 2014.

To cite this article: Sindy Sterckx, Iskander Benhadj, Geert Duhoux, Stefan Livens, Wouter Dierckx, Erwin Goor, Stefan Adriaensen, Walter Heyns, Kris Van Hoof, Gert Strackx, Kris Nackaerts, Ils Reusen, Tanja Van Achteren, Jan Dries, Tom Van Roey, Karim Mellab, Riccardo Duca & Joe Zender (2014) The PROBA-V mission: image processing and calibration, *International Journal of Remote Sensing*, 35:7, 2565-2588, DOI: [10.1080/01431161.2014.883094](https://doi.org/10.1080/01431161.2014.883094)

To link to this article: <http://dx.doi.org/10.1080/01431161.2014.883094>

PLEASE SCROLL DOWN FOR ARTICLE

Taylor & Francis makes every effort to ensure the accuracy of all the information (the "Content") contained in the publications on our platform. However, Taylor & Francis, our agents, and our licensors make no representations or warranties whatsoever as to the accuracy, completeness, or suitability for any purpose of the Content. Any opinions and views expressed in this publication are the opinions and views of the authors, and are not the views of or endorsed by Taylor & Francis. The accuracy of the Content should not be relied upon and should be independently verified with primary sources of information. Taylor and Francis shall not be liable for any losses, actions, claims, proceedings, demands, costs, expenses, damages, and other liabilities whatsoever or howsoever caused arising directly or indirectly in connection with, in relation to or arising out of the use of the Content.

This article may be used for research, teaching, and private study purposes. Any substantial or systematic reproduction, redistribution, reselling, loan, sub-licensing,

systematic supply, or distribution in any form to anyone is expressly forbidden. Terms & Conditions of access and use can be found at <http://www.tandfonline.com/page/terms-and-conditions>

The PROBA-V mission: image processing and calibration

Sindy Sterckx^{a*}, Iskander Benhadj^a, Geert Duhoux^a, Stefan Livens^a, Wouter Dierckx^a,
Erwin Goor^a, Stefan Adriaensen^a, Walter Heyns^a, Kris Van Hooft^a, Gert Strackx^a,
Kris Nackaerts^a, Ils Reusen^a, Tanja Van Achteren^a, Jan Dries^a, Tom Van Roey^a,
Karim Mellab^b, Riccardo Duca^b, and Joe Zender^b

^aFlemish Institute for Technological Research (VITO) – Remote Sensing Unit; ^bESA-ESTEC,
Keplerlaan 1, Noordwijk, The Netherlands

(Received 31 August 2012; accepted 7 February 2013)

With the launch of PROBA-V (Project for On-Board Autonomy – Vegetation) in 2013, the continuity and availability of global land-coverage data in four multispectral bands are ensured for the SPOT (Système Pour l'Observation de la Terre)-VEGETATION user community. This community has been served for already more than 14 years with high-quality 1 kilometre-resolution data. To guarantee continuation of this high quality over the full lifetime of PROBA-V, an operational processing platform and in-flight calibration algorithms have to be in place, which fully consider the specific PROBA-V platform and instrument design characteristics. Data quality has to be ensured for all available product levels, i.e. from the radiometrically corrected radiance data to the 10 day global synthesis. In this article we first focus on some specific design characteristics, which impose some challenges for data processing and calibration. Next, a technical description is given for all the processing steps such as mapping, cloud masking, atmospheric correction, and compositing. The functioning of the Image Quality Centre (IQC) is described. The IQC is in charge of the assessment of the PROBA-V performance, the analysis of the image quality, and the radiometric and geometric calibration after launch. Finally information is given on the distribution of the various products to the user community.

1. Introduction

The PROBA-V (Project for On-Board Autonomy – Vegetation) remote-sensing satellite mission is intended to ensure the continuation of the SPOT 5 VEGETATION products after 2012. The PROBA-V microsatellite is designed to offer a global coverage of land surfaces at four spectral bands at a spatial resolution of 1/3 km and 1 km with a daily revisit for latitudes from +75° N to 56° S.

To cover the wide angular field of view (101°) in a small-sized PROBA platform the optical design of PROBA-V is made up of three cameras (identical three-mirror anastigmatic (TMA) telescopes). Each camera has two focal planes, one for the short wave infrared (SWIR) band and one for the visible and near-infrared (VNIR) bands. The VNIR detector consists of four lines of 5200 pixels. Three spectral bands are selected, compatible with SPOT-VEGETATION (SPOT-VGT): blue, red, and near infrared (NIR). The SWIR detector is a linear array composed of three mechanically staggered detectors of 1024 pixels.

*Corresponding author. Email: Sindy.Sterckx@vito.be

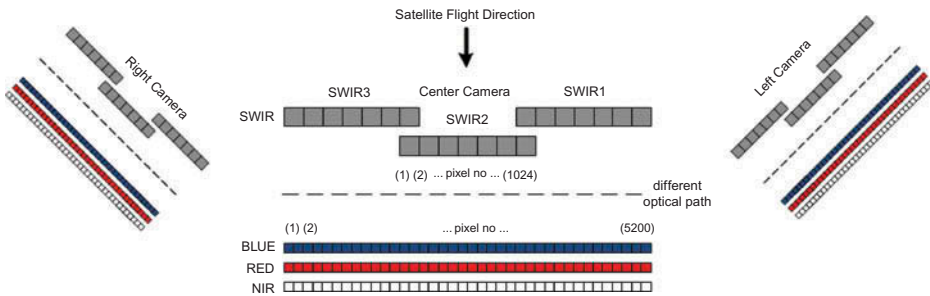


Figure 1. PROBA-V instrument design.

Owing to the separation of the image planes of the different bands, a target on the ground will be observed at slightly different moments in time and under different viewing angles. A target will be first observed by the NIR and about 12 s later by the SWIR detector. The correspondence between instrument design and captured image data is schematically represented in Figure 1.

Based on an on-board stored land-sea mask, each of the three cameras is switched on and off automatically to reduce the consumption of the scarce power and memory. Whereas with the one-camera design of the VGT instrument a SPOT-VGT image segment covers a full instrument swath of 2250 km, a PROBA-V image segment will only cover the swath of one camera.

The larger amount of data due to the increased spatial resolution and the complexity of the PROBA-V instrument design with three separate cameras (independently switched on/off) and staggered SWIR detectors made it necessary to make a full redesign and implementation of the processing facility in use for SPOT-VGT.

The PROBA-V platform and instrument characteristics also impose some major challenges for the in-flight calibration. The constraints on power consumption and the small size and weight of the platform (Dierckx et al. 2014) prevented the availability of on-board calibration devices such as calibration lamps (as available on SPOT-VGT) or solar diffusers such as those used for in-flight calibration of various satellites such as MERIS (Medium Resolution Imaging Spectrometer) and MODIS (Moderate Resolution Imaging Spectroradiometer). Therefore, the PROBA-V in-flight radiometric calibration has to rely solely on vicarious calibration methods outlined in this article. The absence of active thermal control and the distributed cameras (causing a risk of inter-camera differences) further complicate the in-flight radiometric calibration procedures. The characteristics of the PROBA-V satellite which play a major role in the in-flight geometric calibration, are: (1) a payload composed of three-mirror anastigmatic (TMA) cameras; (2) VNIR and SWIR detectors mounted on different locations; (3) VNIR and SWIR with different ground sampling distances (GSDs); (4) mechanically staggered SWIR detector composed of three overlapping detectors with an overlap area; and (5) complex thermo-elastic distortion due to the absence of active thermal control on board.

In this article we will discuss how these challenges are addressed in both ground-processing and calibration strategies in order to guarantee the data product quality for the user. Four topics will be addressed: (1) the PROBA-V data processing, (2) the in-flight radiometric and (3) geometric calibration approach, and (4) the product distribution. This document can then serve as a PROBA-V data-processing reference for future PROBA-V users.

2. Processing chain

The PROBA-V mission objective is to ensure continuity with the heritage of the SPOT-VGT mission. Thus, the PROBA-V mission will continue to provide daily top of canopy (TOC) synthesis (S1-TOC) and 10-day synthesis (S10-TOC) products. In addition, top of atmosphere (TOA) daily synthesis (S1-TOA) products and radiometrically corrected raw data (level 1C) products will also be provided for scientific users.

Within the user segment, the processing facility (PF) chain is designed to generate these products starting from the level 1A data delivered by the data ingestion facility (DIF) (Figure 2). DIF retrieves the data downlinked by the satellite from the secondary ground station and converts it to level 1A. The level 1A product contains the raw uncompressed digital number for each spectral strip together with the telemetry data (satellite position and velocity at 1 Hz and quaternions at 4 Hz) and the line timestamp information. The processing chain is composed of several processing steps as outlined in Figure 2 and briefly detailed in the following sections.

The PROBA-V instrument covers its swath with three cameras. They each independently image narrower areas: about 500 km for the centre camera and about 875 km for the left and right cameras (Figure 3). They slightly overlap in the across-track direction.

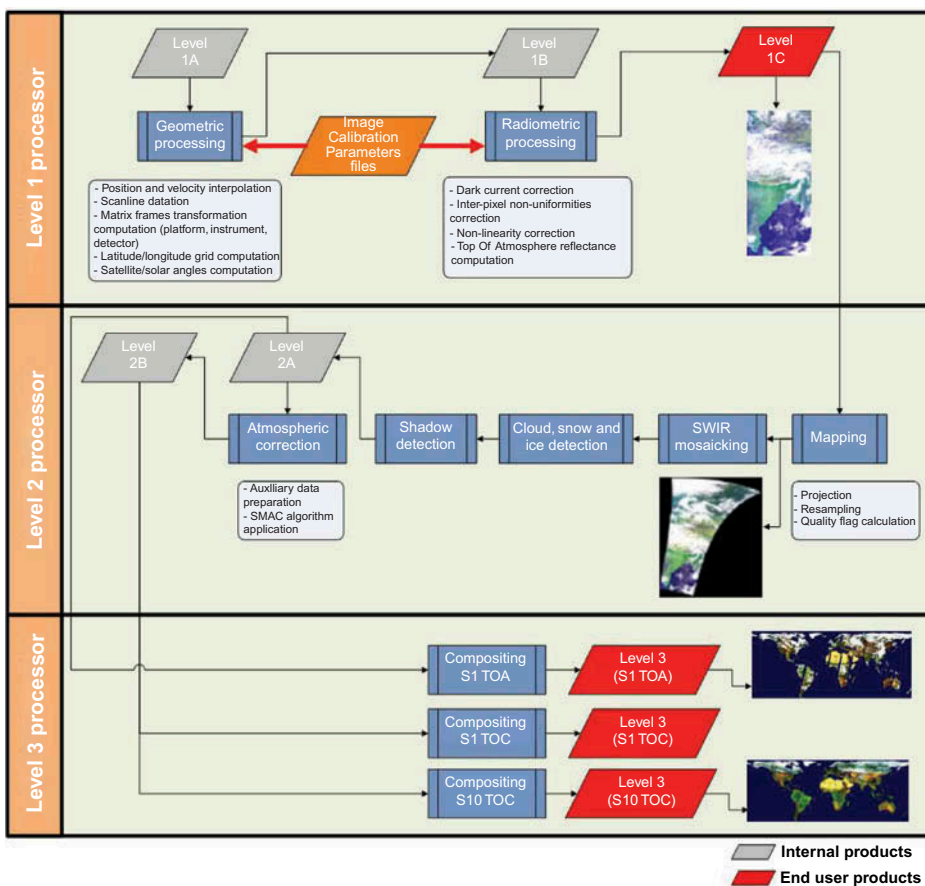


Figure 2. PROBA-V processing facility chart.

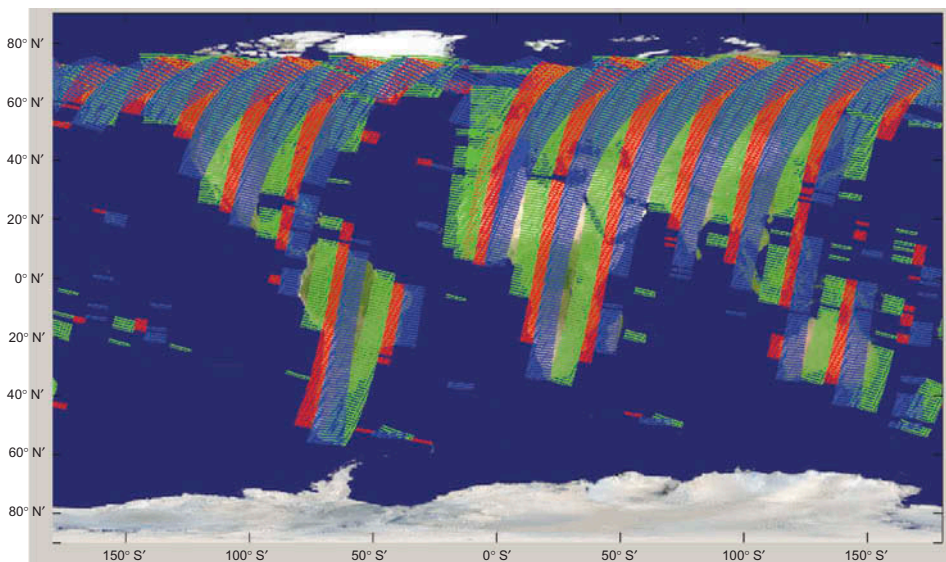


Figure 3. Example of PROBA-V 1 day coverage of the three cameras (1 day orbiting with green = right camera, red = centre camera, blue = left camera).

For the processing, ‘segments’ (i.e. data acquired between a switch on and off of one camera) are not associated with the complete 2250 km swath as is the case for SPOT-VGT, but with the swath of the separate cameras. For the VNIR bands, the raw segments will consist of N lines of 5200 pixels and of 3072 pixels for the SWIR band.

The use of three separate cameras causes an inter-camera co-registration problem. To manage this, the data of the different segments/camera are treated as separate images in all processing steps up to the compositing step (level 3).

The operational workflow takes as input all the segments collected within a given period. The input can consist of a different number of segments of each camera, since all three cameras are autonomously switched on/off independently based on the land–sea mask. For example, during a viewing period Δt we can receive N_1 , N_2 , and N_3 segments from the respective cameras, totalling $N_1 + N_2 + N_3$ (Figure 4). All these segments are given as input to the operational workflow and processed separately up to the compositing step.

Three important processes are defined in the operational workflow (Figure 2). The level 1 processor (see Section 2.1) performs the geometric and the radiometric processing up to the level 1C product. The level 2 processor (see Section 2.2) projects the level 1C product and performs cloud, ice/snow, shadow detection, and atmospheric correction. Finally, the level 3 processor (see Section 2.3) combines all the daily and 10 daily acquisitions to generate the synthesis products.

2.1. Level 1 processor

2.1.1. Geometric processing

For each position of the satellite, a geolocation step is performed to determine the geographical coordinates (latitude, longitude) of the pixel being viewed by the satellite.

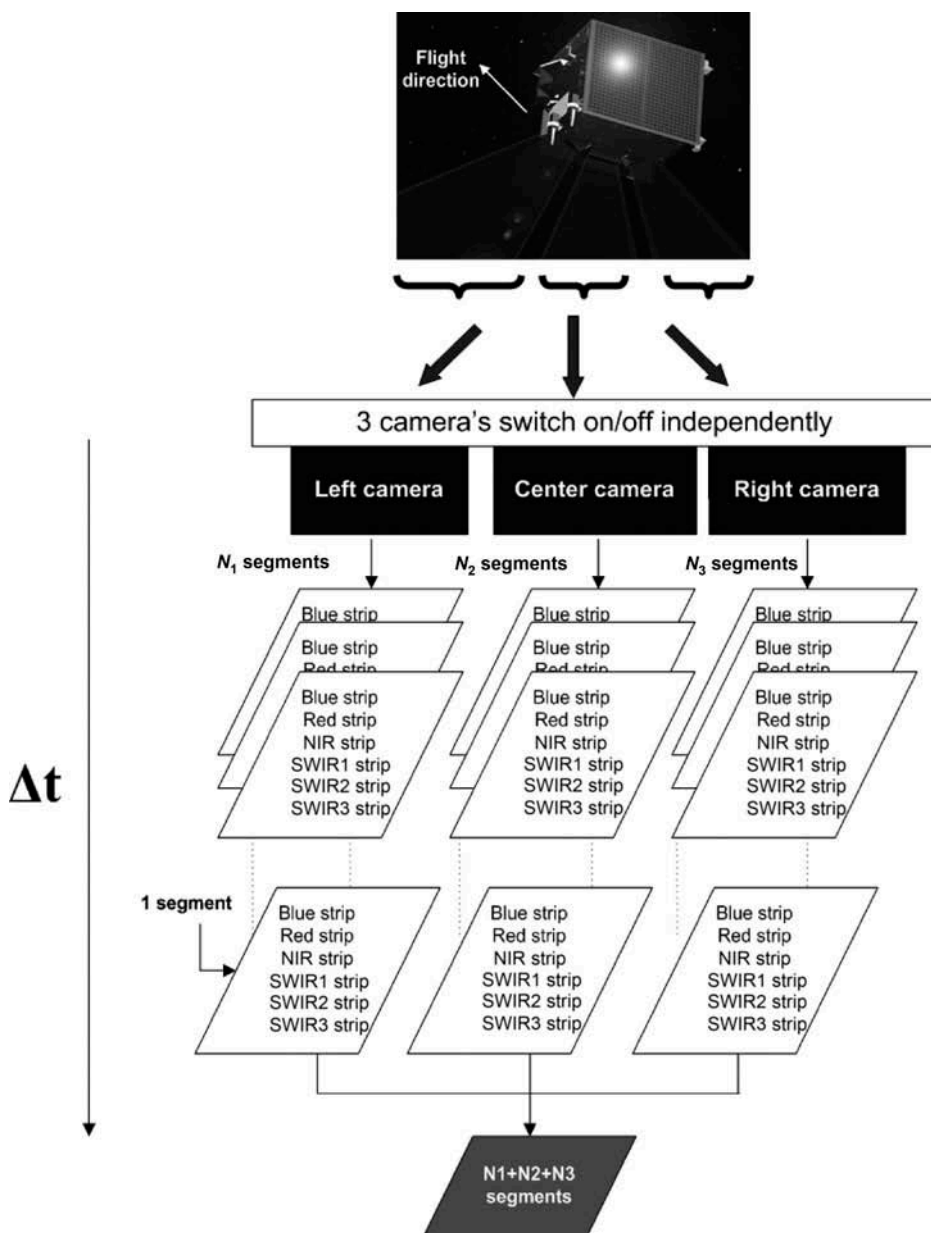


Figure 4. Example of data received within a time period Δt .

This is done at two different heights: 0 m and 5000 m above sea level. This process basically calculates the intersection of satellite viewing direction with an Earth model. The satellite position and velocity are interpolated for each scanline using an orbital propagator model. The scanline's timestamp information is retrieved from level 1A. The different transformation matrices between different reference frames (platform, instrument, detector) are calculated using level 1A's quaternions data together with the polar motion data,

Earth rotation, and precession and nutation data. To refine the geolocation accuracy, the geometric processing model uses the geometric Instrument Calibration Parameters (ICP) file, which is provided and regularly updated by the geometric calibration system (see Section 3.3). The ICP files contain the detector viewing direction variation with respect to the time since out of eclipse (i.e. when the satellite is out of the penumbra) and the Sun beta angle (i.e. the angle between the geocentric position vector to the Sun and the satellite's orbit plane).

In addition, the geometric processing model calculates the necessary solar and satellite viewing angles (zenith and azimuth) needed for further processing. The output of the geometric processing is the level 1B data.

2.1.2. Radiometric correction

This section describes the radiometric processing to be applied to the raw data in order to derive TOA reflectance values. The digital number DN^k for the spectral band k is first corrected for possible non-linearities, dark currents, and inter-pixel non-uniformities, and then converted to at-sensor radiance L^k . The radiance conversion is achieved using the band-specific calibration coefficients derived from the radiometric Instrument Calibration Parameters file provided by the radiometric calibration system (see Section 3.2). Next, the TOA reflectance for each spectral bands k is computed by converting the radiance L^k to TOA reflectance using:

$$\rho_{\text{TOA}}(k) = \frac{\pi \times d^2 \times L^k}{E^k \times \cos(\theta_s^k)}, \quad (1)$$

where $\rho_{\text{TOA}}(k)$ is the TOA reflectance for the spectral band k ; d is the Earth–Sun distance [astronomical units]; E^k is the mean solar exo-atmospheric irradiances for the spectral band k [$\text{W m}^{-2} \text{sr}^{-1}$]; and θ_s^k is the solar zenith angle for the spectral band k [$^\circ$]. The output of the radiometric processing is the level 1C data.

2.2. Level 2 processor

2.2.1. Mapping

A level 2 image is the result of a mapping of (a number of bands) of a level 1 image to a given user projection grid. The Plate Carrée projection is used for all PROBA-V products to preserve the continuity with the SPOT-VGT products. In the mapping procedure (Riazanoff 2004), first the inverse model is used to determine for a given pixel at location (x, y) in the level 2 data grid its corresponding (p, l) coordinates in the level 1 data (Figure 5). This is performed using a polynomial predictors function that relates the (x, y) to the (p, l) coordinates. This operation is performed twice (for the latitude/longitude grid at 0 m and 5000 m) resulting in two sets of (p, l) coordinates $(p, l)^0 \text{ m}$ and $(p, l)^{5000 \text{ m}}$. Then it is possible to calculate for each pixel the correct (p, l) coordinates given the corresponding height by means of linear interpolation. The digital elevation model (DEM) used to perform the orthorectification is the Global Land Survey Digital Elevation Model (GLSDEM) from NASA and the USGS.

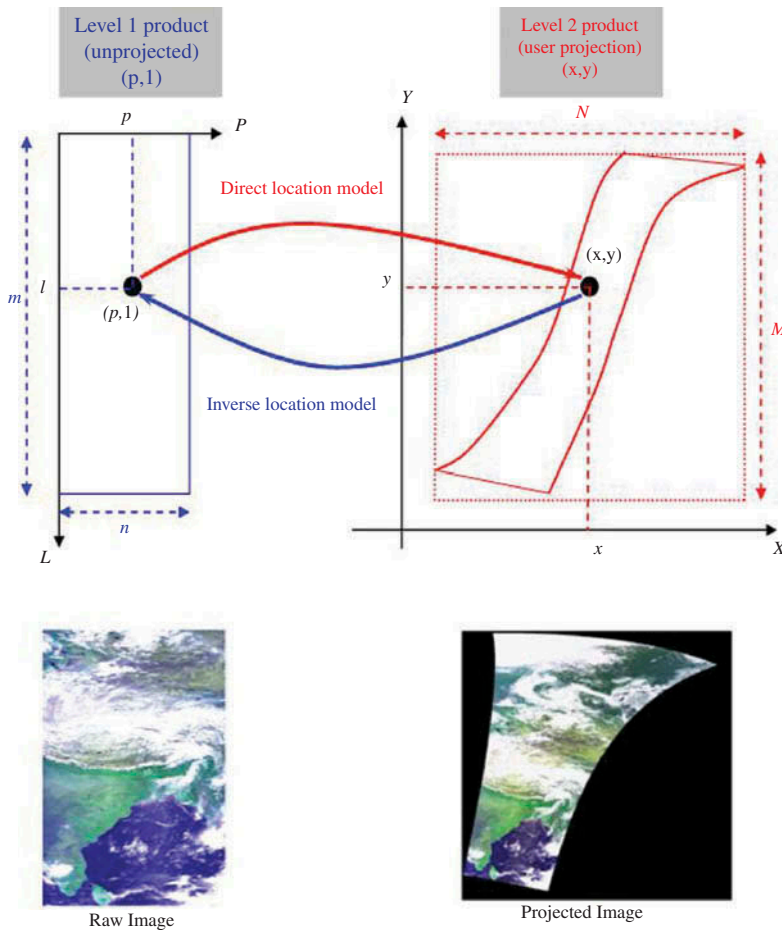


Figure 5. Mapping procedure.

Once the (p, l) coordinates are known, for each band of level 2 data the pixel value to be mapped can be determined using a stretched bi-cubic interpolation filter (Dierckx et al. 2014). The standard bi-cubic filter using four neighbouring grid points is a re-sampling algorithm with high-quality smoothing for target grids with the same or less dense spacing as the original grid (which was the case for SPOT-VGT). However, this method is not suitable for PROBA-V data because of the strong pixel size variation across track (Figure 6) (from 100 m at nadir to 350 m at the edges of the swath for the VNIR bands and 200–700 m for the SWIR band). The stretched bi-cubic filter is found to be more suitable in our case and tends to give good results (Dierckx et al. 2014).

2.2.2. SWIR mosaicking

The SWIR detector of each camera is composed of three strips. After the mapping step, there are still three projected SWIR strips. A mosaicking step is applied to build the SWIR

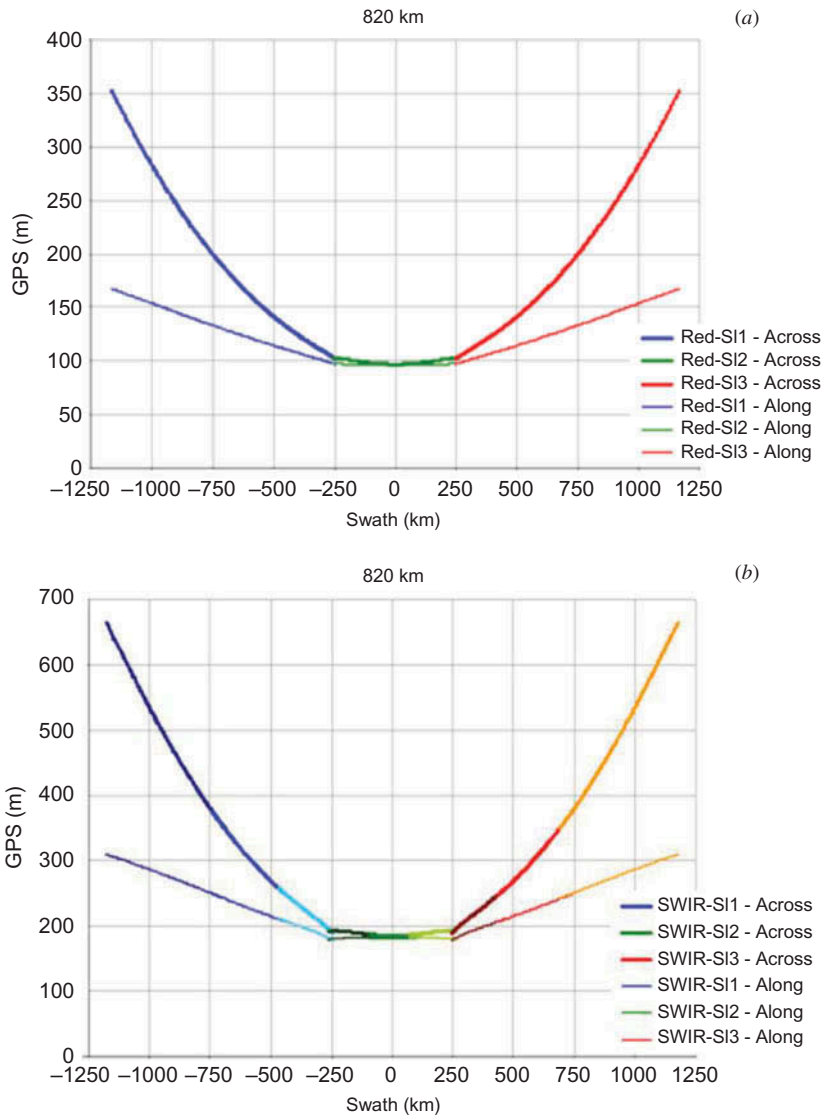


Figure 6. Ground pixel size (GPS) as a function of across-track distance on the ground for the red channel (a) and the SWIR channel (b) (source OIP, Versluys et al. (2012)). The flight altitude was 820 km in both cases.

band. In the strip overlapping regions (Figure 7) the pixel radiometric status map is taken into account to select the best pixel.

2.2.3. Cloud detection

Clouds obstruct the viewing of the Earth's surface by satellites operating in the visual and infrared spectrum. Based on their particular spectral behaviour, they can be detected and eliminated from the image before further processing. Cloud detection is an essential part of the preprocessing chain for various value-added products of the PROBA-V satellite.

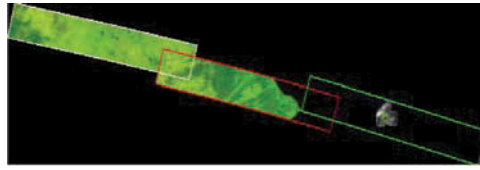


Figure 7. Example of the result of the mosaicking algorithm of the three SWIR strips.

Cloud detection for VGT was based on a simple multiple threshold rule applied to the blue and SWIR spectral bands (Lisens et al. 2000). In this algorithm, cloud detection is performed on the projected segment (level 2) with the assumption that a cloud is in the same position in the blue and SWIR bands.

This algorithm could not simply be taken over because of the instrument design difference with PROBA-V. PROBA-V has different detectors/strips with different viewing direction planes (Figure 8). The NIR detector is the first to see the cloud and about 12 s later the SWIR detector is the last to see it. As the figure illustrates, SWIR and NIR will map the cloud into different positions on Earth. For a cloud at a height of 7 km the two positions are more than 500 m apart vertically.

The cloud detection algorithm developed for PROBA-V also uses both blue and SWIR bands. It creates two masks: the first one is based on a threshold on the blue band with an additional check on the SWIR band. The second is based on a threshold on the SWIR band with an additional check on the blue band. The final mask is simply the result of merging of the two masks.

The shift that can be caused by the difference in the viewing direction between the blue and SWIR bands ($d_4 + d_3$ see Figure 9) combined with the shift due to wind speed will not exceed three pixels along track and one pixel across track (in both directions left and right).

The algorithm (Figure 10) checks whether the value of the pixel in the blue band is higher than the blue threshold and whether the maximum of the SWIR values in a 3 pixel \times 3 pixel-window above the same blue pixel in the image is higher than the SWIR threshold (see Figure 10). If these two conditions are satisfied, the blue pixel is classified

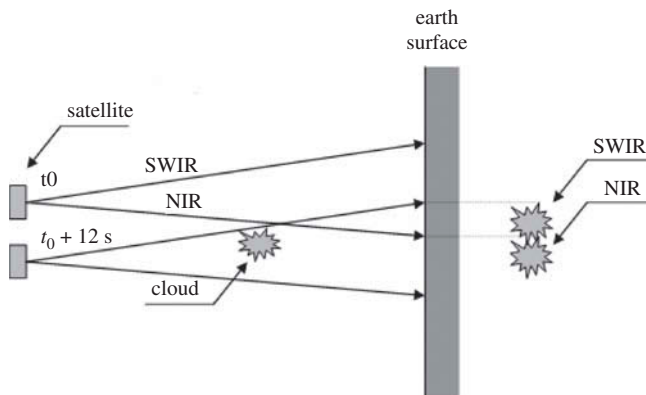


Figure 8. Cloud detection problem statement.

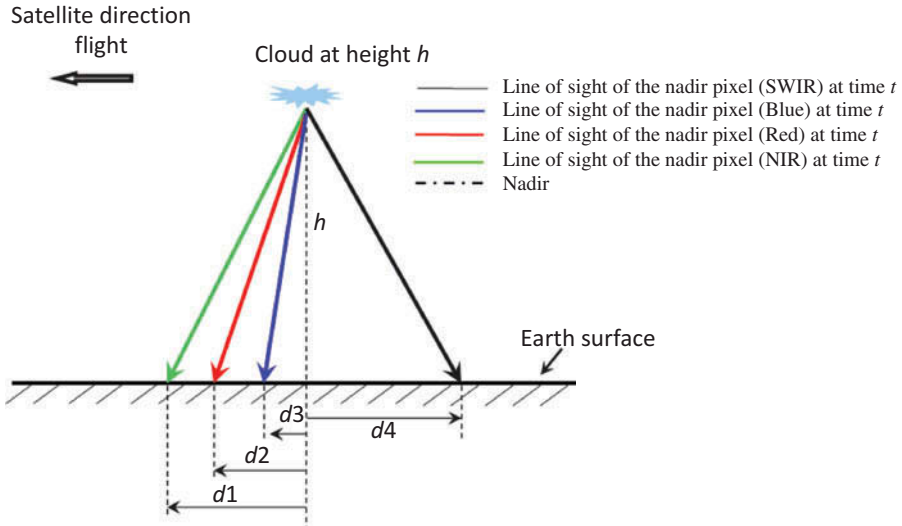


Figure 9. Shifts in cloudy pixels due to the difference in viewing direction of all spectral bands.

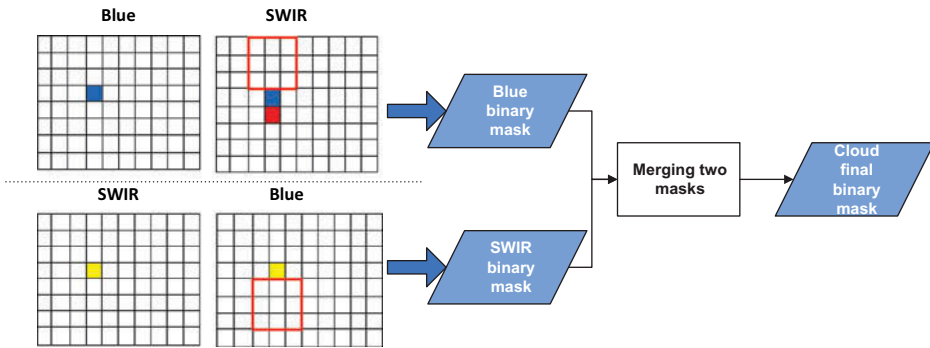


Figure 10. Cloud detection process.

as cloudy. The cloudy pixels in the NIR band are mostly located in front of the cloudy pixels in the blue band image (Figure 10). Thus, the pixel below the cloudy blue pixel in the image is also classified as cloudy. The same above-mentioned procedure is applied on the SWIR band, but with an additional forward window (3×3) check in the blue band (Figure 10). The result of merging both masks is a binary mask (0 = clear and 1 = cloudy).

2.2.4. Snow/ice detection

The Snow/Ice detection algorithm used is the one of the SPOT-VGT mission (Lisens et al. 2000). The binary snow mask is generated using thresholds on some derived indices (Equation (2)) calculated from the TOA reflectance of the four spectral bands.

$$\left\{ \begin{array}{l} S_1 = \rho\text{TOA}(\text{RED}) \\ S_2 = \rho\text{TOA}(\text{SWIR}) \\ S_3 = \frac{\rho\text{TOA}(\text{BLUE}) - \rho\text{TOA}(\text{NIR})}{\rho\text{TOA}(\text{BLUE}) + \rho\text{TOA}(\text{NIR})} \\ S_4 = \frac{\rho\text{TOA}(\text{BLUE}) - \rho\text{TOA}(\text{SWIR})}{\rho\text{TOA}(\text{BLUE}) + \rho\text{TOA}(\text{SWIR})} \\ S_5 = \frac{\rho\text{TOA}(\text{BLUE}) + \rho\text{TOA}(\text{RED})}{2} - \rho\text{TOA}(\text{SWIR}). \end{array} \right. \quad (2)$$

Figure 11 shows the scheme of the snow decision diagram.

2.2.5. Shadow detection

In land applications of satellite remote sensing, not only cloud but also cloud-shadow is regarded as a source of errors and thus a shadow mask needs to be generated. Many

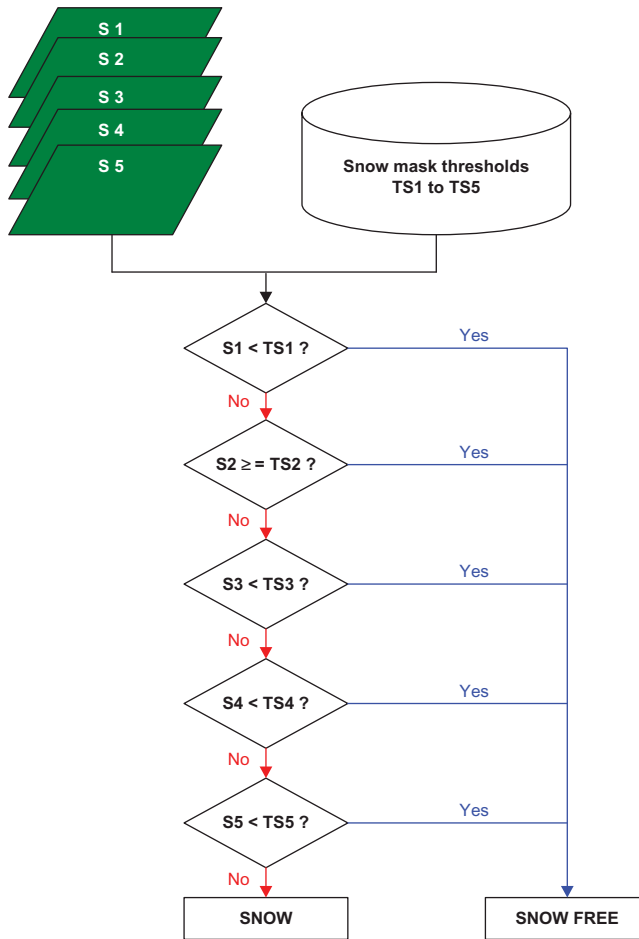


Figure 11. Snow decision tree.

studies dealing with cloud-shadow problems exist. Three main types of methods exist in the literature: (1) radiometric approaches based on some conditions on the reflectance (thresholding, ratio, etc.) as used in the MODIS shadow detection (Ackerman et al. 2006), (2) geometric approaches using a Sun–cloud–sensor geometry model to retrieve the shadow pixel (Simpson, Jin, and Stitt 2000), and (3) methods based on analysis of satellite time series data (Simpson and Stitt 1998).

The selected PROBA-V algorithm uses a technique that combines the radiometric and the geometric methods to provide a cloud-shadow mask, as proposed in Lisens et al. 2000. The geometric model is presented in Figure 12. The cloud pixel (p) is located at the centre, although the actual cloud is at height h from the tangential plane (intersection of the sunbeam and the line of sight from the satellite to the cloud pixel). The shadow pixel can be found as the intersection of the sunbeam and the tangential plane at the centre. The solar zenith and solar azimuth angles are assumed equal in the cloud and shadow pixels. Let φ be the angle between the meridian north (taken as the x -axis) and the vector from the cloud and the shadow pixel. In Figure 12, it is shown that φ equals the sum of γ (positive or negative according to the relative azimuth angle) and the viewing azimuth angle. (For the definition of γ , see Equation (4).)

The position of the shadow pixel is fixed when r (distance between cloud pixel and associated shadow pixel) (Figure 12) and φ are known. Using geometry, they are calculated as

$$r = h \sqrt{\tan^2 \theta_s + \tan^2 \theta_v - 2 \tan \theta_v \tan \theta_s \cos \phi_R}, \quad (3)$$

$$\varphi = \underbrace{\pm \cos^{-1} \left(\frac{\tan \theta_v - \tan \theta_s \cos \phi_R}{\tan^2 \theta_s + \tan^2 \theta_v - 2 \tan \theta_v \tan \theta_s \cos \phi_R} \right)}_{\gamma} + \phi_{av}. \quad (4)$$

Cloud heights are predicted by making use of radiometric information of the TOA reflectance. Starting from the cloud pixel p and tracing the NIR radiance along the projected path from cloud to shadow in the image (see Figure 13), a relative change (or gradient) of NIR band reflectance is detected. In the presence of shadow, a maximum to minimum transition corresponds in general to the cloud edge and shadow edge, respectively. If the relative change $\Delta B3$ is above a threshold (typically 20%), a shadow edge is

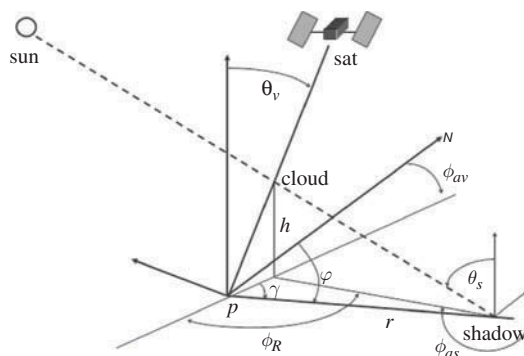


Figure 12. Geometric model.

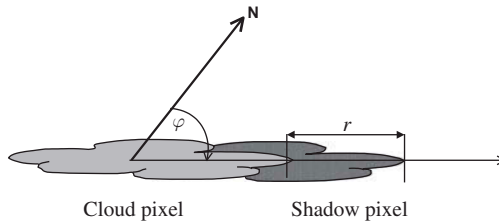


Figure 13. Potential shadow pixels are found by tracing radiances along the path cloud→shadow.

detected. The respective locations of the cloud and shadow edge will thus be used to calculate the cloud height (Equation (3)).

Shadows are then calculated using a Sun–target–sensor geometry model. These shadow pixels are then checked on the cloud mask, because the cloud could cover the shadow, in which case the shadow pixel is rejected. The resulting pixels that are not in the cloud mask are still subject to a check on radiometry. This smoothes away the errors due to (non-shadow→vegetation) transitions such as rivers, shadows of mountains, and bright surfaces. This whole process results in a binary mask (0 = clear and 1 = shadow).

2.2.6. Atmospheric correction

Data acquired by optical sensors are perturbed by scattering and absorption due to gases and aerosols. An atmospheric correction is a prerequisite step for retrieving bi-directional surface reflectances. To ensure data continuity with the SPOT-VGT mission, the Simple Model for Atmospheric Correction (SMAC) code (version 4.2) is used (Rahman and Dedieu 1994). It converts the TOA reflectance into TOC reflectance (ρ^{TOC}). To achieve this conversion, SMAC needs some auxiliary data as input (water vapour, ozone, surface pressure, etc.). Estimates of meteorological models for the water vapour content are obtained from MeteoServices (<http://www.meteoservices.be>). Pressure is derived from the DEM. Aerosol quantities are estimated using an optimization algorithm applied to the blue spectral band (Maisongrande et al. 2000).

2.3. Level 3 processor

The level 3 processor performs the composition. The purpose of this step is to combine, in an optimal manner, multiple observations over a given time interval into a single and cloud-free synthesis image. This operation starts from atmospherically corrected images and takes into account the variation in residual clouds, and the sensor view and Sun angle conditions. The compositing steps minimize the cloud coverage (by discarding cloudy pixels), angular variations, and maximizes the global coverage. This allows depicting spatial and temporal variations in vegetation.

Another reason to perform S10 compositing is to avoid spatial coverage gaps. Owing to the fact that daily descending PROBA-V orbits do not completely overlap, especially at the equator, at least two orbiting days are needed to obtain global coverage. Data discontinuity might also be caused by calibration campaigns conflicting with the nominal acquisitions or possible problems in data transmissions at the reception station.

The atmospherically corrected segments are combined to a global synthesis at level 3. A maximum value composite (MVC) (Tarpley, Schneider, and Money 1984; Holben

1986) approach is used to select the pixel with the maximum normalized difference vegetation index (NDVI). This approach will select the cloud-free pixels. To ensure the continuity of VGT products, the compositing period is the same as VGT. The following two synthesis products are generated.

- S1(1-day synthesis) product is generated every day.
- S10 are decadal syntheses with as start dates the 1st, 11th, or 21st of a month.

The compositing rules, i.e. the rules to select the ‘best’ observation, are as follows.

- An observation covered by all spectral band is preferred over a pixel covered by only a few bands.
- An observation for which the pixel quality is good for all bands is preferred over a pixel with bad radiometric values.
- A ‘clear’ observation is preferred over an ‘ice/snow’ observation, which itself is preferred over a ‘cloud’ observation.
- In case of two observations satisfying the previous rules, the viewing and solar angles of both observations are compared following some thresholding rules. Observations with angles lower than a minimum threshold are considered as ‘good’, and observations with angles higher than a maximum threshold are considered as ‘bad’. Observations with angles between both thresholds are considered as ‘acceptable’. A ‘good’ observation is preferred over ‘acceptable’ observation, which itself is preferred over a ‘bad’ observation. A selection based on the viewing and solar angles reduces the influence of atmospheric contamination and residual cloud since pixels acquired with the smallest solar zenith angle have the lowest optical path length.
- If two observations still satisfied all the above-mentioned rules, an observation with the maximum NDVI is preferred.

3. Calibration and validation

3.1. Calibration phases and objectives

Careful in-lab pre-launch calibration and characterization under operating environmental conditions, such as space temperature and vacuum, and the full range of possible viewing conditions are essential (1) to ensure that related mission requirements are met over the sensor’s range of operating conditions, (2) to minimize the risk of bringing to light undiscovered problems after launch and therefore to promote mission success, and (3) to provide calibration/characterization datasets that cannot be obtained in flight. Radiometric and spectral performance characteristics that will be verified on ground are: signal-to-noise ratios, dark currents, linearity, stray light, pixel non-uniformity, polarization sensitivity, spectral response, and spectral misregistration. Geometric performance characteristics include modulation transfer function (MTF), bore sight, and spatial misregistration.

The assessment of the PROBA-V performance, the analysis of the image quality, and the calibration after launch will be performed by the PROBA-V Image Quality Center (IQC) located at the Flemish Institute for Technological Research (VITO). The calibration/validation (CAL/VAL) commissioning phase will start after the platform and instrument verification and validation phase (first three months) and is scheduled to be a three-month activity. The objectives of the Cal/Val activities during the commissioning phase are: (1) to verify instrument performance after launch, (2) to check for instabilities

of the radiometric calibration with respect to temperature or other driving parameters, (3) to perform in-flight instrument radiometric calibration, (4) to validate that the calibration meets the absolute and relative accuracy requirements, (5) to deliver at the end of the commissioning phase this calibration in the form of the ICP file, and (6) to update the Cal/Val plan for the operational phase to start at the end of the commissioning phase for the whole duration of the mission. The Cal/Val objectives of the operational phase are: (1) to continuously monitor the instrument calibration parameters and performance in order to be able to compensate for drifts caused by systematic changes such as ageing of the instruments and (2) to update the ICP file as needed to maintain the accuracy of the calibration and continuity of product quality.

As the satellite has no on-board calibration facility, vicarious calibration techniques are used to monitor sensor performance over time. Special calibration acquisitions with specific instrument settings (e.g. decreased integration time (IT)) and/or over non-nominal sites (e.g. oceans) will be requested through the IPC (Instrument Programming Center). The IPC allows capturing the requests for the instrument, to plan them in relation with the flight dynamics, to validate them against resources constraints, to send them to the Mission Control Center (MCC), and to monitor their uploading and execution.

3.2. In-flight radiometric calibration

3.2.1. The sensor radiometric model

The sensor radiometric model defines the relation between the raw digital output, which is registered by the sensor and sent down for data processing, and the derived effective spectral radiance assumed to be present at the sensor. Taking into account possible non-linearities in sensor response, the relationship between digital output and effective radiance can be written as

$$DN_j^k / NL(DN_j^k) = A^k \cdot g_{j,m}^k \cdot G_m^k \cdot L_j^k + dc_{j,m}^k, \quad (5)$$

where the superscript k and subscript j identify, respectively, the spectral band and the pixel. DN is the raw digital output, A is the absolute calibration coefficient, L is the effective radiance, G is the gain, m is the gain number, dc is the dark current, g is the detector's pixel relative sensitivity or equalization coefficient, and NL is the non-linearity function, common for all the detector's pixels.

Initial values for these parameters are given by the on-ground calibration. Degradation of these parameters after launch is expected due to ageing of the optical parts. Therefore the IQC will supply, when needed, the user segment processing facility with new calibration parameters for the processing of the raw images in a file named the ICP file. The level 1C (and higher-level data) will contain in its metadata file full traceability to the used ICP file. These ICP files will be available to end-users through the same distribution channels as the end-products.

3.2.2. The vicarious radiometric calibration plan

For every parameter of Equation (5), specific image acquisitions and (combination of) methods will be employed. An overview of these methods is given in Figure 14.

Dark current (dc_{im}^k) is caused by thermally generated electrons that build up in the detector's pixels. The magnitude of the dark current is expected to increase with time due

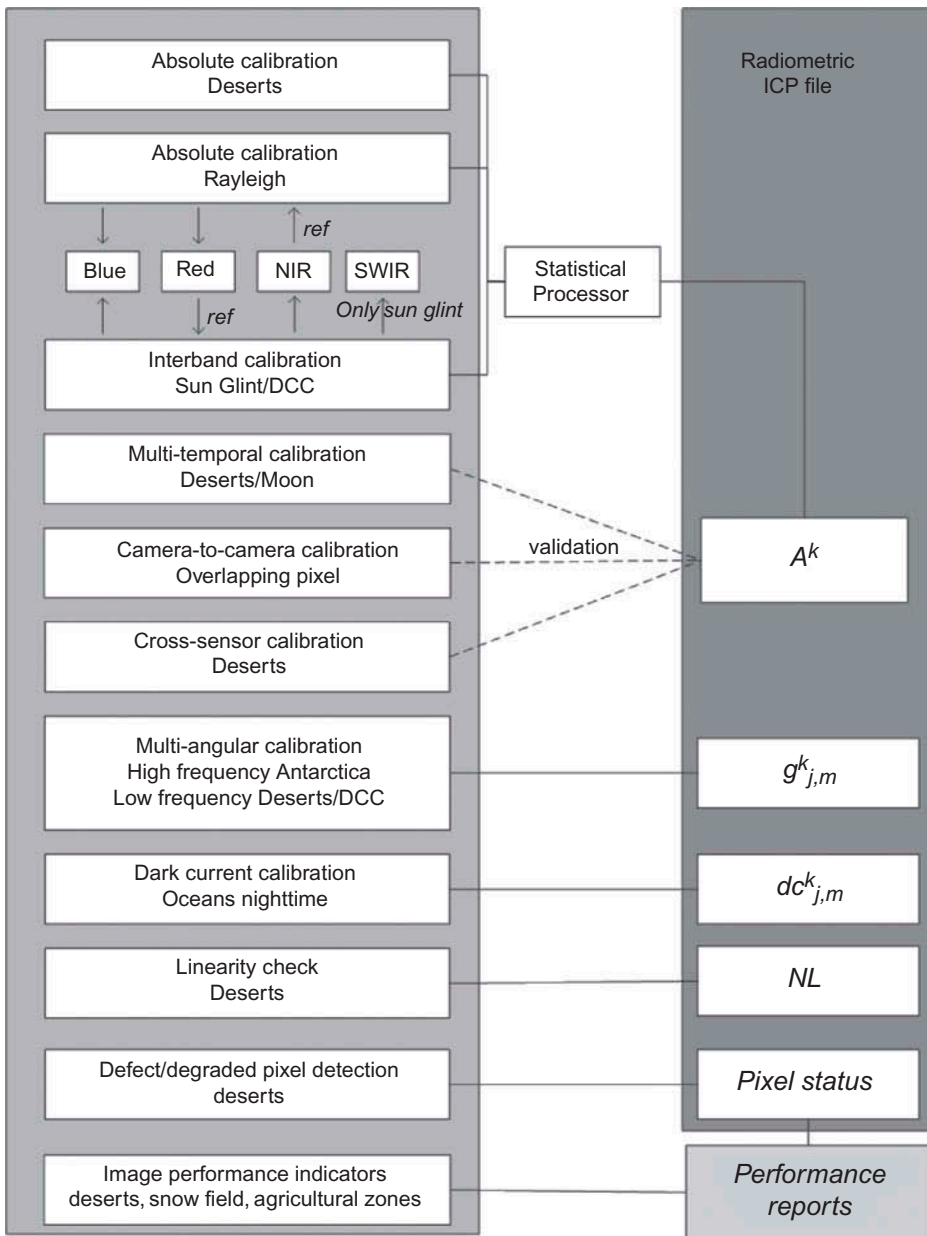


Figure 14. Radiometric Cal/Val plan for the PROBA-V mission.

to space radiation. Moreover, noticeable variations of dark current are expected over the course of the year as a result of temperature effects. It is therefore important to monitor the dark current in orbit. Images taken during the night-time portion of the orbit over dark ocean sites will be used to determine the dark current values for all pixels. Images should be taken during night in uncompressed mode preferably in a prolonged image capture mode, where the IT can be extended as far as 10 s.

The measurement of the linearity of the relation between effective spectral radiance and digital output is crucial, as systematic deviations from this linearity may occur in flight. Possible causes of this are saturation of the sensor because of surface full well (interface traps capturing electrons) saturation and/or saturation of the electronics because of voltage cut-off. In-flight linearity tests will be performed by changing the IT while imaging homogenous bright targets.

To meet and verify after launch the radiometric calibration requirements for PROBA-V, specified at 5% for the absolute accuracy and at 3% for the relative accuracy (inter-band, multi-temporal, and camera-relative) (Dierckx et al. 2014), several independent absolute and relative calibration approaches will be used. Furthermore, the combination of methods allows reducing uncertainty in the results, independently validating results, and determining and accounting for systematic errors in one or more techniques.

The optical sensor calibration with simulated radiance (OSCAR) facility is developed for the routine vicarious calibration of PROBA-V. One of the implemented absolute vicarious calibration methods is based on the use of TOA simulations over bright desert surfaces as an absolute reference (Govaerts, Sterckx, and Adriaensen 2013). The use of an advanced radiative transfer model that accounts for polarization, the improvement of the surface reflectance characterization, and the use of a non-spherical aerosol model increased significantly the accuracy achievable by the method originally developed by Govaerts and Clerici (2004). Validation of the approach using various satellite data (i.e. Aqua-MODIS, MERIS, AATSR (Advanced Along-Track Scanning Radiometer), PARASOL (Polarization and Anisotropy of Reflectances for Atmospheric Sciences coupled with Observations from Lidar) and SPOT-VGT) extracted from ESA Database for Imaging Multi-spectral Instruments and Tools for Radiometric Intercomparison (DIMITRI) (<http://www.argans.co.uk/dimitri/>) has shown that absolute calibration over the Libya-4 desert is achievable with this approach with an accuracy of 3% (Govaerts, Sterckx, and Adriaensen 2013). Acquisitions over desert calibration sites are part of the nominal operations and therefore they are subject to the nominal dynamic IT matrix with ITs depending on the solar zenith angles (Dierckx et al. 2014). Detailed simulations have been carried out to mitigate any saturation over land targets.

For the operation calibration of the blue and red PROBA-V bands the so-called Rayleigh calibration approach (Vermote et al. 1992; Fougnie et al. 2007) is also implemented and throughout validated (Sterckx, Livens, and Adriaensen 2013). The primary assumption of the approach is that the ocean does not contribute to the TOA signal in the NIR (Gordon and Wang 1994). The assumption holds for Case 1 (Morel and Prieur 1977) waters with low chlorophyll concentration and where phytoplankton is the only optically significant water column contributor. Rayleigh or molecular scattering can accurately be calculated based on the surface pressure and viewing angles. The contribution of aerosol scattering can be derived from the NIR reference band where molecular scattering is negligible. The aerosol content estimated from the NIR band is then transferred to the blue and red band to model the TOA radiance with a radiative transfer code. The simulated radiance values are then compared with the measured values to derive the absolute calibration coefficient. To reduce the perturbing part of the signal due to ocean reflectance and the presence of foam, strict pixel selection procedures are used. Pixels can only be chosen within oligotrophic areas with well-known weak and stable chlorophyll contents. Suitable oligotrophic Rayleigh calibration zones have been identified by Fougnie et al. (2002). Morel, Claustre, and Gentili (2010) have reported monthly averaged chlorophyll concentrations for these oligotrophic areas. Special calibration acquisitions will be scheduled to acquire images over these oceanic sites with an increased IT setting.

The results obtained with the Rayleigh method can be transferred to other bands (NIR, SWIR) based on inter-band calibration approaches such as deep convective clouds (DCC) (for the NIR band) and Sun glint (for both NIR and SWIR).

The DCC approach uses bright, thick, high-altitude, convective clouds over oceanic sites. Their reflective properties are spectrally flat in visible and near-infrared and the only contributions to the observed signal are from the cloud reflectance, molecular scattering, and ozone absorption, which can be modelled with a radiative transfer code. Using the red band as reference (assumed to be well calibrated by the Rayleigh approach) to retrieve cloud optical thickness, the blue and NIR band can be calibrated (Lafrance et al. 2002). Details on the implementation can be found in Sterckx, Livens, and Adriaensen (2013). The method is not suited for the SWIR band as clouds are no longer spectrally uniform in this spectral region. Calibration images over DCC will be taken with short IT settings to minimize risk of saturation. Calibration acquisitions during the operational phase will not be performed for the orbits for which land data is in the swath so as not to impact the nominal operations.

Throughout validation of the Rayleigh, deep convective clouds methods on the basis of SPOT-VGT 1 and VGT 2 combined with theoretical error budget estimations have shown that the mission requirement specifications for radiometric calibration, i.e. 5% absolute and 3% relative (inter-band, cross-sensor), are realistic achievable goals for the PROBA-V mission despite the absence of on-board calibration devices (Sterckx, Livens, and Adriaensen 2013).

This Sun glint method uses the specular reflection of the Sun on the ocean surface. This Sun glint reflection is high and spectrally flat and is used to transfer the absolute calibration of one reference band to other spectral bands (inter-band calibration) (Hagolle et al. 2004; Fournie et al. 2007). The size of the Sun glint spot is variable as it depends on the ocean surface roughness, which is controlled by wind speed. Owing to the chosen local time (around 10h30) of the descending node in the Sun-synchronous orbit of PROBA-V, Sun glint is always observed in the eastern direction. Therefore, without platform manoeuvres Sun glint calibration can only be performed for the eastern- and middle-looking cameras (depending on location and day of the year) because their viewing direction is close to the exact specular direction.

The combination of the results obtained with the different methods into suitable operational calibration coefficients will be performed following a statistical methodology. This approach allows for handling results obtained from various techniques and combines them in a hierarchical scheme into the overall best estimates for the calibration coefficients. The method is based on the precise handling of accuracies in accordance with the ISO Guide to the Expression of Uncertainty in Measurement (GUM) (expression of uncertainty in measurements) (JCMG 2008).

Inter-band calibration is defined by reference to band k_0 as

$$A^{k.k_0} = A^k / A^{k_0}. \quad (6)$$

The inter-band calibration accuracy is the accuracy of the estimate for $A^{k.k_0}$. Inter-band calibration accuracy will be assessed using images over Sun glint spots and deep convective clouds. Deep convective clouds allow assessing the inter-band calibration accuracy of blue and NIR bands with respect to the red band. It cannot however be used for the SWIR band. The Sun glint calibration approach is, on the other hand, also suitable for the SWIR band.

The multi-temporal calibration coefficient, which tracks the instrument degradation at time t by reference to an initial time t_0 , is defined as

$$A_{t,t_0}^k = A_t^k / A_{t_0}^k. \quad (7)$$

The multi-temporal calibration accuracy is the accuracy of the estimate for A_{t,t_0}^k . Multi-temporal calibration accuracy will be assessed using images over stable desert sites; furthermore, the use of lunar observations for instrument stability monitoring is under investigation. Calibration over stable deserts has the advantage of allowing daily acquisitions throughout the year without impacting the routine mission.

As the calibration methods treat the three PROBA-V cameras separately, to minimize inter-camera deviations, a camera-to-camera calibration method is used based on the overlap area between two adjacent cameras. The camera-to-camera calibration method can deliver a continuous check with respect to the temporal evolution of the radiometric calibration coefficients of the different cameras and allows detecting biases between cameras.

The multi-angular equalization coefficients current ($g_{j,m}^k$) describes the sensitivity variations of the imager over the field or view. Slow variations due to the optical system are characterized on ground and validated in flight using the absolute calibration results obtained with Rayleigh, DCC, and absolute desert approaches over the field of view. The sensors themselves can exhibit high-frequency variations between detector pixels, which will be estimated in flight from images taken from snow-covered areas over Antarctica or Greenland. As the homogeneous areas are small compared to the swath of the camera, results over a set of images are combined in a robust manner to cover the complete field of view, resulting in an accurate equalization profile, which can be used to effectively remove unwanted striping from the images.

The instrument's image quality in flight is assessed in terms of instrumental noise and image contrast on ground targets. To determine instrumental noise effects on the measured signals, ground targets should be spectrally uniform over the measured range; hence, targets such as desert zones or snow zones are considered. To determine image contrast, carried out here by measuring the instrument system MTF, ground targets should have regions of high contrast. The technique of two-image comparison is used, which is a common technique used for instruments with lower spatial resolutions. For this technique, targets should have regions of high contrast; in addition, the distribution of brighter and darker regions should contain a spread of spatial frequencies (Li, Gu, and Yu 2009). Agricultural zones are chosen as ground targets that fulfil this requirement (as was done for MODIS in Rojas, Schowengerdt, and Biggar 2002).

3.3. In-flight geometric calibration

The in-flight geometric calibration for PROBA-V has been discussed in Mica et al. 2012. First, the TMA design does not comply with a pinhole sensor model behaviour as illustrated in Adriaensen et al. (2010). Second, the complex thermo-elastic properties due to the absence of active thermal control on board poses a major challenge: the absence of active temperature control implies that the temperature can play a major role in the geometric calibration process. Thus, a traditional sensor model will not be adequate and a highly specific geometrical calibration model is needed. This is supported by the fact that

the TMA design (Versluys et al. 2012) implies that the focal lengths are somewhat different for every pixel in the focal plane.

Hence, we propose modelling the CCD viewing direction vectors directly for each pixel. This is carried out by a general polynomial model. An 8th order of polynomial coefficient for both along-track and across-track deformations is used to describe the CCD distortions with respect to the nominal ICP of the central camera in the focal plane geometry. This approach provides the possibility of compensating for complex distortions related to the specific and novel TMA camera design. This approach is also used by Leica for their three-line ADS40 scanner (Tempelmann, Hinsken, and Recke 2003). Simulations presented in Mica et al. 2012 indicate that an 8th order polynomial is sufficient to reach the accuracy requirements when a ground control point (GCP) matching an accuracy of 0.25 pixel is achieved. Table 1 summarizes the calibration parameters to be extracted.

The in-flight geometric calibration for PROBA-V is discussed in Mica et al. 2012. The complex thermo-elastic properties due to the absence of active thermal control on board pose a major challenge: the absence of active temperature control implies that temperature can play a major role in the geometric calibration process. Thus, a quite complex geometrical calibration model is needed. This was studied using the PROBA-V thermo-elastic model (TEM). It shows that sensor deformations are expected to follow the solar flux, which could not be linked to a single temperature model during on-ground simulations. Instead it can be modelled by a periodic component within the orbit (time since out of eclipse – TOE) and a slow change of deformation with time (seasonal variation of the Sun beta angle).

Both these changes are carefully modelled by the geometric calibration system. It will estimate and monitor regularly the exterior orientation parameters (bore-sight angles) and interior orientation deformations (CCD viewing direction vectors) of each camera of the PROBA-V sensor using a vast amount of ground control points, spread all over the globe, extracted from the Landsat GeoCover 2000 dataset. These geometrical calibration parameters shall be used to update (nominally every 4 weeks) the geometric ICP file used by the processing facility, to guarantee the geometrical accuracy of the system-corrected products reported in Table 2. The whole geometric calibration procedure is highly automatic. This will allow processing of large volumes of data with limited human intervention.

The estimation of the interior and exterior parameters is performed via a weighted and constrained inversion model, which is based on an iterative least squares adjustment. It is noted that a strong correlation may exist between parameters and not all parameters can be estimated simultaneously. However, the interior and exterior orientations need not be determined separately. On the contrary our objective is to estimate a combination of them

Table 1. Calibration parameters. The VNIR sensor contains three detector arrays each corresponding to a single strip, and the SWIR sensor contains a single detector array made up of three strips.

Calibration parameters	Number of parameters
Exterior orientation parameters:	
Boresight angle for each camera	3 (angles) \times 3 (cameras)
Interior orientation parameters:	
8th degree polynomial model for each camera and strip for along-track and across-track	8 \times 3 (cameras) \times 6 strips 8 \times 3 (cameras) \times 6 strips

Table 2. PROBA-V geometric accuracy requirements. ‘Goal accuracy’ means an accuracy of 95% and ‘mandatory accuracy’ means an accuracy of 95%.

Geo-localization measurements	Goal accuracy (m)	Mandatory accuracy (m)
Inter-band (VNIR)	100	
Inter-band (SWIR + VNIR)	150	300
Multi-temporal (VNIR)	150	
Multi-temporal (SWIR + VNIR)	225	500
Absolute (VNIR)	300	
Absolute (SWIR + VNIR)	450	1000

in order to guarantee the requested geometrical system accuracy. In addition, correlated parameters may lead to singular (not invertible) least square normal equations. The unified least squares method (Mikhail, Bethel, and McGlone 2001) is proposed, which introduces an *a priori* weight for each calibration parameter. These weights act as a regularization method (e.g. the Tikhonov regularization method, Tychonoff and Arsenin (1977)) avoiding singularities in the modified normal equation.

An automatic ground control point (GCP) extraction method based on a local interest operator, called Modified Moravec Interest Operator (USGS), is proposed. It allows generating a geometric reference dataset containing a large number of high-quality (e.g. with corners, distinctive edges, etc.) GCPs regularly spread over the land. The GCP chips database covering the entire Earth has been extracted from the Landsat GeoCover 2000 dataset in a fully automatic way. Image correlation is used to match ‘interest points’ of GCP chips. Ma, Chan, and Canters (2010) indicated image matching accuracies better than 0.5 pixels and on average better than 0.25 pixels for a similar matching approach with multi-angular images.

The adopted calibration strategy consists in extracting the calibration parameters (exterior and interior orientations) from the geometric calibration at single scene basis and then performing weighted constrained least square fits, in terms of Sun beta angle and time since out of eclipse, of the resulting series of measures (one for each scene) in order to generate the final calibration parameter trends. The scene size is a compromise: it needs to be small enough so that the orientation parameters can be considered constant within the scene, and at the same time large enough so that a reasonable estimate of the parameters can be made. The TEM analysis and the estimation of the average number of GCPs showed that an 800 km along-track acquired segment is a good choice. This was adopted as the standard scene size. During the calibration campaign, several scenes with similar time out of eclipse and Sun beta angle values will be processed. The final calibration parameters will have a reduced error, owing to a weighted averaging effect, with respect to parameters extracted from a single scene.

A set of predefined geographic regions of interest (ROIs) over the land covering approximately 6° of latitude and going from 180° W to 180° E and from 80° N to 56° S is chosen for the scene geometric calibration. It is expected that approximately 100 level 1C scenes per camera every 4 days shall be processed. Since the nominal geometric calibration campaign period is 4 weeks, in order to assemble enough scenes spread over the Earth taking into account cloudy days, a total amount of approximately 700 scenes per camera are processed for generating the calibration parameters. It is important to point out that a scene is useful within the above process only if a minimum number of GCPs can be extracted from a scene. Sea, cloud, and snow coverage will obviously reduce the number

of GCPs found in a scene because in these places the algorithm will not find any match between the imagery and the GCPs.

4. Product distribution

Within the user segment, the product distribution facility allows users to discover, view, order, and download products. The available product types consist of the following.

- Level 1C, S1-TOA, S1-TOC, and S10-TOC products from the PROBA-V mission. The synthesis products are provided both in 1 km and 1/3 km spatial resolution and in Plate Carrée projection. The level 1C products are provided in raw resolution. The file format is HDF5 (Hierarchical Data Format), but for specific users other formats such as HDF4 (SPOT-VGT product format) and GeoTIFF can be provided. The synthesis products will be provided in granules of $10^\circ \times 10^\circ$, owing to the large product sizes of the global products.
- ICP files and calibration reports from the PROBA-V mission for scientific users.
- Related data, e.g. historical products from the SPOT-VGT missions and derived higher-level products from these missions.

A user can use the Web-based interface to query products from the catalogue and view the metadata and quicklook(s) of the products. Products can be immediately downloaded from the Web portal or products can be ordered, which will become available to the user via FTP or an HTTP URL. The user will be notified via e-mail or can use the order overview on the Web portal. Furthermore, a user can subscribe to get future products immediately when they become available.

The product distribution facility is highly customizable according to the needs of different product types. User-customized products that are included in the system are e.g. the selection of specific bands, the clipping according to a region of interest (ROI), or requesting a mosaic of multiple granules. These can be offered towards specific users according to an authorization policy. Medium-term storage is available to provide fast access to the most recent products; older products can be retrieved from the long-term archive automatically when users request their access. VITO is also aiming to develop an open-source toolbox which will allow experienced users to perform with their own computing resources a customization on clipping, band selection, and projection (in the case of unprojected level 1C data).

In addition to the Web-based interface, which will be operated by VITO, a GSCDA (GMES Space Component Data Access) (<http://gmesdata.esa.int/web/gsc/about-gsc-data-access>)-compliant interface is developed, which allows users to discover and order PROBA-V products through the ESA GSCDA service. This channel will provide access to the PROBA-V synthesis products S1-TOA, S1-TOC, and S10-TOC in the native format and in 1 km spatial resolution towards the GMES community.

5. Summary

The PROBA-V processing facility and image quality center are designed to generate different image products with an image quality meeting the radiometric and geometric requirements throughout the mission lifetime. The radiometric calibration requirements for PROBA-V specify 5% absolute accuracy and 3% relative accuracy (inter-band, multi-temporal, and camera-relative). The increased geometric resolution (i.e. 1/3 km vs. 1 km

for SPOT-VGT) imposed more stringent requirements regarding geo-localization. To reach these requirements, the specific PROBA-V instrument and platform properties were taken into account in both calibration process and image processing. These are the very large swath realized by three TMA cameras, the separation of the images planes of the different VNIR and SWIR detectors, the mechanically staggered SWIR detector, and the absence of active thermal control and on-board calibration devices. In this article PROBA-V users will find the necessary background information on the image processing steps and on the Cal/Val plan set-up for the mission to ensure product data quality.

Acknowledgements

The authors acknowledge the contribution of the teams from Qinetiq Space, OIP, Spacebel, ACS, Trasys. This work was supported by Belpo and ESA (PROBA-V User Segment contract 091669).

References

- Ackerman, S., K. Strabala, P. Menzel, R. Frey, C. Moeller, L. Gumley, B. Baum, S. Wetzel, S. Seemann, and H. Zhang. 2006. "Discriminating Clear-Sky from Cloud with MODIS Algorithm Theoretical BASIS Document (MOD35)." *Version 5.0*: 129.
- Adriaensen, S., I. Benhadj, G. Duhoux, W. Dierckx, J. Dries, W. Heyns, R. Kleihorst, S. Livens, K. Nackaerts, I. Reusen, S. Sterckx, T. Van Achteren, and J. Everaerts. 2010. "Building a Calibration and Validation System for the PROBA-V Satellite Mission." *Proceedings EuroCOW 2010 Int. Cal. and Orient. Workshop*, Castelldefels, February 10–12.
- Dierckx, W., S. Sterckx, I. Benhadj, G. Saint, S. Livens, G. Duhoux, T. Van Achteren, M. Francois, and K. Mellab. 2014. "PROBA-V Global Vegetation Satellite: Review of the Upcoming Mission." *International Journal of Remote Sensing* 35.
- Fougnie, B., G. Bracco, B. Lafrance, C. Ruffel, O. Hagolle, and C. Tinel. 2007. "PARASOL In-Flight Calibration and Performance." *Applied Optics* 46 (22): 5435–5451.
- Fougnie, B., P. Henry, A. Morel, D. Antoine, and F. Montagner. 2002. "Identification and Characterization of Stable Homogeneous Oceanic Zones: Climatology and Impact on In-flight Calibration of Space Sensor over Rayleigh Scattering." *Proceedings of Ocean Optics XVI*, Santa Fe, November 18–22.
- Gordon, H. R., and M. Wang. 1994. "Retrieval of Water-Leaving Radiance and Aerosol Optical Thickness Over the Oceans with SeaWiFS: A Preliminary Algorithm." *Applied Optics* 33: 443–452.
- Govaerts, Y. M., and M. Clerici. 2004. "Evaluation of Radiative Transfer Simulations Over Bright Desert Calibration Sites." *IEEE Transaction on Geoscience and Remote Sensing* 42 (1): 176–187.
- Govaerts, Y. M., S. Sterckx, and S. Adriaensen, 2013. "Use of Simulated Reflectances Over Bright Desert Target as an Absolute Calibration Reference." *Remote Sensing Letters* 4 (6): 523–531.
- Hagolle, O., J. M. Nicolas, B. Fougnie, F. Cabot, and P. Henry, 2004. "Absolute Calibration of VEGETATION Derived from an Interband Method Based on the Sun Glint Over Ocean." *IEEE Transactions on Geoscience and Remote Sensing* 42 (7): 1472–1481.
- Holben, B. N. 1986. "Characteristics of Maximum-Value Composite Images from Temporal AVHRR Data." *International Journal of Remote Sensing* 7: 1417–1434.
- JCMG. 2008. *Guide to the Expression of Uncertainty in Measurement, ISO/IEC Guide 98-3:2008*. Geneva: International Organization for Standardization.
- Lafrance, B., O. Hagolle, B. Bonnel, Y. Fouquart, and G. Brogniez. 2002. "Interband Calibration Over Clouds for POLDER Space Sensor." *IEEE Transactions on Geoscience and Remote Sensing* 40 (1): 131–142.
- Li, X. Y., X. F. Gu, and T. Yu. 2009. "In-Flight MTF Measurement and Compensation for the CBERS-2 WFI." *International Journal of Remote Sensing* 30 (4): 829–839.
- Lisens, G., P. Kempeneers, F. Fierens, and J. Van Rensbergen. 2000. "Development of Cloud, Snow, and Shadow Masking Algorithms for VEGETATION Imagery." *Proceedings of Geoscience and Remote Sensing Symposium, IGARSS 2000, Honolulu, HI* 2: 834–836.

- Ma, J., J. C.-W. Chan, and F. Canters. 2010. "Fully Automatic Subpixel Image Registration of Multiangle CHRIS/Proba Data." *IEEE Transactions on Geoscience and Remote Sensing* 48 (7): 2829–2839.
- Maisongrande, P., B. Duchemin, G. Dedieu, and M. Leroy. 2000. "A New Algorithm for Atmospheric Correction of Surface Reflectances Delivered by the VEGETATION System." *Proceedings of Geoscience and Remote Sensing Symposium, IGARSS 2000, Honolulu, HI* 2: 24–28.
- Mica, S., L. Galli, G. Duhoux, S. Livens, V. Jovanovic, A. Giustiniani, J. Dries, J. Zender, and S. Santandrea. 2012. "PROBA-V Geometric Calibration." *Proceedings IGARSS 2012, Munich*, July 22–27.
- Mikhail, E. M., J. S. Bethel, and J. C. McGlone, 2001. *Introduction to Modern Photogrammetry*, 479p. New York: John Wiley and Sons.
- Morel, A., H. Claustre, and B. Gentili. 2010. "The Most Oligotrophic Subtropical Zones of the Global Ocean: Similarities and Differences in Terms of Chlorophyll and Yellow Substance." *Biogeosciences Discuss* 7: 5047–5079.
- Morel, A., and L. Prieur. 1977. "Analysis of Variations in Ocean Color." *Limnology and Oceanography* 22 (4): 709–722.
- Rahman, H., and G. Dedieu. 1994. "SMAC: A Simplified Method for the Atmospheric Correction of Satellite Measurements in the Solar Spectrum." *International Journal of Remote Sensing* 15: 123–143.
- Riazanoff, S. 2004. *SPOT123-4-5 Satellite Geometry Handbook, GAEL-P135-DOC-001, 1, Revision 4*, p. 82.
- Rojas, F., R. A. Schowengerdt, and S. F. Biggar. 2002. "Early Results on the Characterization of the Terra MODIS Spatial Response." *Remote Sensing of Environment* 83 (1–2): 50–61.
- Simpson, J. J., Z. Jin, and J. R. Stitt, 2000. "Cloud Shadow Detection Under Arbitrary Viewing and Illumination Conditions." *IEEE Transactions on Geoscience and Remote Sensing* 38: 972–976.
- Simpson, J. J., and J. R. Stitt, 1998. "A Procedure for the Detection and Removal of Cloud Shadow from AVHRR Data Over Land." *IEEE Transactions on Geoscience and Remote Sensing* 36: 880–897.
- Sterckx, S., S. Livens, and S. Adriaensen. 2013. "Rayleigh, Deep Convective Clouds and Cross Sensor Desert Vicarious Calibration Validation for the PROBA-V Mission." *Transactions on Geoscience and Remote Sensing* 51 (3): 1437–1452.
- Tarpley, J. P., S. R. Schneider, and R. L. Money. 1984. "Global Vegetation Indices from NOAA-7 Meteorological Satellite." *Journal of Climate Applied Meteorology* 23: 491–494.
- Tempelmann, U., L. Hinsken, and U. Recke. 2003. "ADS40 Calibration & Verification Process." *Proceedings of the ISPRS WG1/5 International Workshop, Castelldefels, September 22–23*.
- Tychonoff, A. N., and V. Y. Arsenin. 1977. *Solution of Ill-Posed Problems*. Washington, DC: Winston & Sons.
- USGS Publications Warehouse. *Extraction of GCP Chips from GeoCover Using Modified Moravec Interest Operator (MMIO) Algorithm*. The United States Geological Survey (USGS) Online Repository. http://landsat.usgs.gov/documents/MMIO_GeoCover_Control_White_Paper.pdf
- Vermote, E., R. Santer, P. Y. Deschamps, and M. Herman. 1992. "In-Flight Calibration of Large Field of View Sensors at Short Wavelengths Using Rayleigh Scattering." *International Journal of Remote Sensing* 13 (18): 3409–3429.
- Versluys, J., D. Kendall, W. Moelans, D. Mollet, P. Holbrouck, D. Vrancken, D. Taccola, and M. Francois. 2012. "The Vegetation Instrument: A Small Scale High Performance Earth Observation Instrument." *Proceedings of Small Satellite Systems and Services – The 4S Symposium, Portorož, June 4–8*.